Journal of Magnetism and Magnetic Materials 560 (2022) 169665

Contents lists available at ScienceDirect

Journal of Magnetism and Magnetic Materials

journal homepage: www.elsevier.com/locate/jmmm

Research article

The emergence of kπ skyrmions and their spin wave modes in a ferromagnetic disk

H. Vigo-Cotrina [a,*], D.L. Monteiro [b], J.P.V. Urruchua [b], A.P. Guimarães [c]

[a] Departamento de Ciencias, Universidad Privada del Norte, Trujillo, Peru
[b] PROVOC - Centro Brasileiro de Pesquisas Físicas, 22290-180, Rio de Janeiro, RJ, Brazil
[c] Centro Brasileiro de Pesquisas Físicas, 22290-180, Rio de Janeiro, RJ, Brazil

ARTICLE INFO

Keywords:
Skyrmion
Target skyrmion
Skyrmionium
Micromagnetic simulation
Spin waves
Hysteresis

ABSTRACT

Using micromagnetic simulations, we show that varying the perpendicular anisotropy constant K_z and the Dzyaloshinskii–Moriya exchange constant D_{int} one can stabilize kπ skyrmions (k =1, 2, … 5) in a ferromagnetic nanodisk. We have studied their spin wave modes, and obtained the spatial profile of the radial and azimuthal modes, for different values of D_{int}. Hysteresis curves and the variation of the skyrmion topological charges were obtained as a function of the value of a planar applied magnetic field. The curves show how the application of the field induces the conversion between different kπ skyrmions.

1. Introduction

Skyrmionic textures in ferromagnetic nanostructures have gained interest in recent years [1–14].

Unlike the simple skyrmion (k = 1), the spatial profile of the kπ skyrmions (k > 1) has additional out-of-plane domains [1,2].

A 2π skyrmion can emerge in thin cylindrical and polygonal geometries [12,14], and recently Yang et al. [3] showed that it can also be formed in hemispherical shells.

A kπ skyrmion has topological charge $|Q| = 1$ for k odd and Q = 0 for k even. Due to this property, for example, a 2π skyrmion (skyrmionium), with $Q = 0$, can move without suffering deflections induced by the skyrmion Hall effect (SkHE), and it can reach higher velocities when compared to a simple skyrmion [15], properties relevant to applications in Spintronics.

The study of the spin wave modes is an important issue, due to their applications in magnonics [16]. Spin wave modes can be used in the process of creating and switching 2π skyrmions [3,17–19] and in signal processing and transmission [6,20,21].

Spin wave modes for a simple skyrmion have been studied by several authors [22–26]. Additionally, the stability of kπ skyrmions (k $\geq$ 2) in a ferromagnetic nanodisk has only been studied as a function of a perpendicular magnetic field [27], Dzyaloshinskii–Moriya interaction [28] and mechanical strains [29]. Thus, the knowledge of the influence of the perpendicular uniaxial anisotropy and the Dzyaloshinskii–Moriya interaction on the stability and spin wave modes of kπ skyrmions is still lacking. Thus, the main goal of this work is to study the influence of the Dzyaloshinskii–Moriya interaction (DMI) on the ground state of a ferromagnetic nanodisk and on the spin wave modes. The other problem that we have investigated is the variation of the magnetization and stability of the kπ skyrmions submitted to a cycle of planar magnetic fields.

2. Results and discussion

The micromagnetic simulations were performed using the open source code Mumax3 [30].

A cobalt cylindrical ferromagnetic layer with diameter D = 150 nm and thickness L = 1 nm, coupled to a nonmagnetic layer, was simulated. The ferromagnetic layer was discretized in 1 × 1 × L nm^3 size cells. Typical parameters of cobalt were used [10–14]: saturation magnetization $M_s = 5.8 \times 10^5$ A/m, exchange stiffness $A_{ex} = 15$ pJ/m and damping constant $\alpha = 0.3$. In order to reduce staircase effects due to the circular geometry, we have used a value of edgesmooth parameter equal to 8. We have used values of perpendicular uniaxial anisotropy constant K_z and D_{int} ranging from 0.50 MJ/m^3 to 1.5 MJ/m^3 and from 0 mJ/m^2 to 7 mJ/m^2, respectively. [10–14]. The range of possible D_{int} values is an open question in the literature. Theoretical works, using ab-initio calculations, predict that it is possible to obtain large values of D_{int} in the systems Co/NM, NM/Co/NM multilayers, where NM is a nonmagnet [31–33]. For example, in Ref. [32], using ab-initio calculations it is shown that higher values of D_{int}, of approximately

* Corresponding author.
E-mail address: helmunt.vigo@upn.edu.pe (H. Vigo-Cotrina).

https://doi.org/10.1016/j.jmmm.2022.169665
Received 12 March 2022; Received in revised form 17 June 2022; Accepted 26 June 2022
Available online 28 June 2022

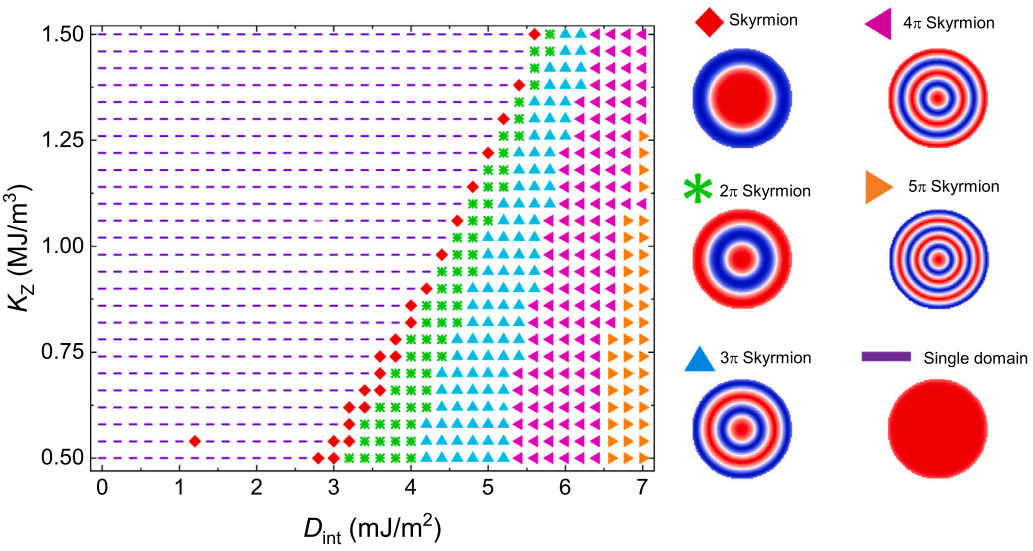

Fig. 1. Phase diagram of the ferromagnetic nanodisk obtained from micromagnetic simulations.

6 mJ/m^2, can be obtained when cobalt is between a nonmagnetic material and an insulator (e.g., MgO/Co/Pt). Using electric fields, values of just over 7 mJ/m^2 can be obtained. However, experimental results for similar systems show lower values, of approximately 2.5 mJ/m^2 [34]. This difference can be attributed to the disordered interface and grain structure due to the fabrication process of the nanostructure, e.g., in the case of sputtered thin films, as mentioned in Ref. [32].

The first step was to obtain a phase diagram (Fig. 1) showing the ground state of the cylindrical ferromagnetic layer. This phase diagram was obtained for zero magnetic field. For this purpose, in our simulations, we have considered six initial magnetic configurations: perpendicular single domain and kπ skyrmion (for k = 1, 2, …, 5). For each initial magnetic configuration it was obtained its respective final magnetic configuration. The values of the energies of these final configurations were compared in order to obtain the lowest value, which corresponds to the ground state of the nanodisk. This stage was repeated for each combination of parameters (K_z, D_{int}). The results of this stage are shown in the phase diagram in Fig. 1.

In Fig. 1, it is possible to observe that kπ skyrmions emerge for values of D_{int} ranging from 2.8 mJ/m^2 to 7 mJ/m^2 for K_z = 0.50 MJ/m^3. However, when K_z increases up to K_z = 1.50 MJ/m^3, that range is reduced to values of D_{int} between 5.6 mJ/m^2 and 7 mJ/m^2. This behavior is expected, due to the fact that the perpendicular anisotropy aligns the magnetic moments in the z-direction, favoring the perpendicular single domain configuration. On the other hand, for a fixed value of K_z, we can see that k increases with the increase of D_{int}, due to the fact that the Dzyaloshinskii–Moriya interaction favors the twisting of the magnetic moments, leading to the formation of skyrmions with extra out-of-plane domains. Note that, for K_z > 1.22 MJ/m^3, it was not possible to obtain a 5π skyrmion.

We have measured the diameters[1] of the cores of the kπ skyrmions for all values of D_{int} used in this work, where it was possible to obtain them (not necessarily as the ground state of the disk). These values are shown in Fig. 2. In all cases, it is possible to observe a smooth increase in the values of the diameters with the increase of the values of D_{int}. It is possible that due to the Dzyaloshinskii–Moriya interaction, the energy of the domain wall regions is reduced, favoring the increase of the out-of-plane domains. Of course, the diameters of the cores are limited by the diameter of the disk.

The next step was to obtain the power spectra of the spin wave modes of the kπ skyrmions[2] (for k = 2, …, 5) as a function of D_{int}. For that, we have chosen a fixed value of K_z = 0.8 MJ/m^3 and a range of values of D_{int} in which it is possible to obtain the desired kπ skyrmion (not necessarily as the ground state of the disk). The simulation starts by considering a kπ skyrmion as initial magnetic configuration for the nanodisk and allowing it to relax. After that, in order to excite the spin wave modes, a sinc magnetic field pulse $B_z = B_0 Sinc(2\pi f_c(t-t_0))$ (for radial modes) and $B_x = B_0 Sinc(2\pi f_c(t-t_0))$ (for azimuthal modes) was applied, where B_0 = 5 mT is the magnetic field intensity, f_c is the cut-off frequency and t_0 = 1 ns is the time delay. The temporal evolution of the spatial profiles (considering all cells of the nanodisk) of the z-component and x-component of the magnetization were stored every 5 ps for a total of 10 ns. For this stage a lower damping constant α = 0.01 was used, in order to obtain a better resolution of the spin wave modes.

Each power spectrum was obtained performing a fast Fourier transform (FFT) from the temporal evolution of the spatial profile (considering all cells of the nanodisk) of the z-component (for radial modes), and x-component of the magnetization (for azimuthal modes). The power spectra for radial spin wave modes[3] of the kπ skyrmions (k = 2, 3, 4 and 5), as a function of D_{int} are shown in Fig. 3

In Fig. 3 we can see that in a general way, the values of the frequencies of the radial spin wave modes increase with the increase of D_{int}. The values of the frequencies for the minimum and maximum value of D_{int} are shown in the Supplementary Material.

In order to gain more information about the spin wave modes, the spatial distribution profiles of the amplitudes of FFT and phases of the oscillation of the spin wave modes (see Fig. 4) were obtained. The oscillations occur within the walls that bound the Skyrmions. Thus, these regions determine the position of the rings of the oscillations. Also, these regions are narrow, and consequently, the rings are also narrow. The width of these regions is of approximately 5 nm.

2π skyrmion:

For mode 1, the oscillation amplitudes of the radial spin wave modes are distributed in two rings around the center of the disk (D_{int} = 3.3 mJ/m^2). The outer diameter formed by the maximum oscillation amplitude has a larger intensity than the inner diameter formed by

[1] In the Supplementary Material are shown the definitions of D_1, D_2, D_3, D_4 and D_5.

[2] We have not considered k = 1, because this case has been well studied. See for example Refs. [3,23–25,35].

[3] The fourth mode for a 4π and 5π skyrmion is not described because it appears in a shorter range of values of D_{int}.

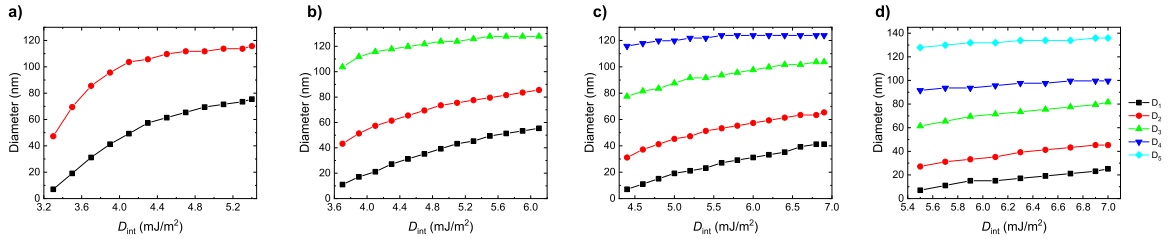

Fig. 2. Diameters of the kπ skyrmions as a function of the D_{int} constant, (a) for a 2π skyrmion, (b) for a 3π skyrmion, (c) for a 4π skyrmion and (d) for a 5π skyrmion.

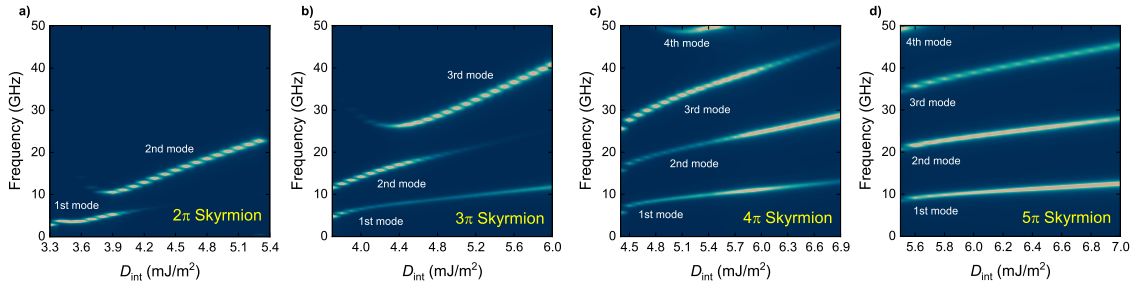

Fig. 3. Power spectra of the kπ skyrmions as a function of the Dzyaloshinskii–Moriya exchange constant D_{int} for radial modes, (a) for a 2π skyrmion, (b) for a 3π skyrmion, (c) for a 4π skyrmion and (d) for a 5π skyrmion.

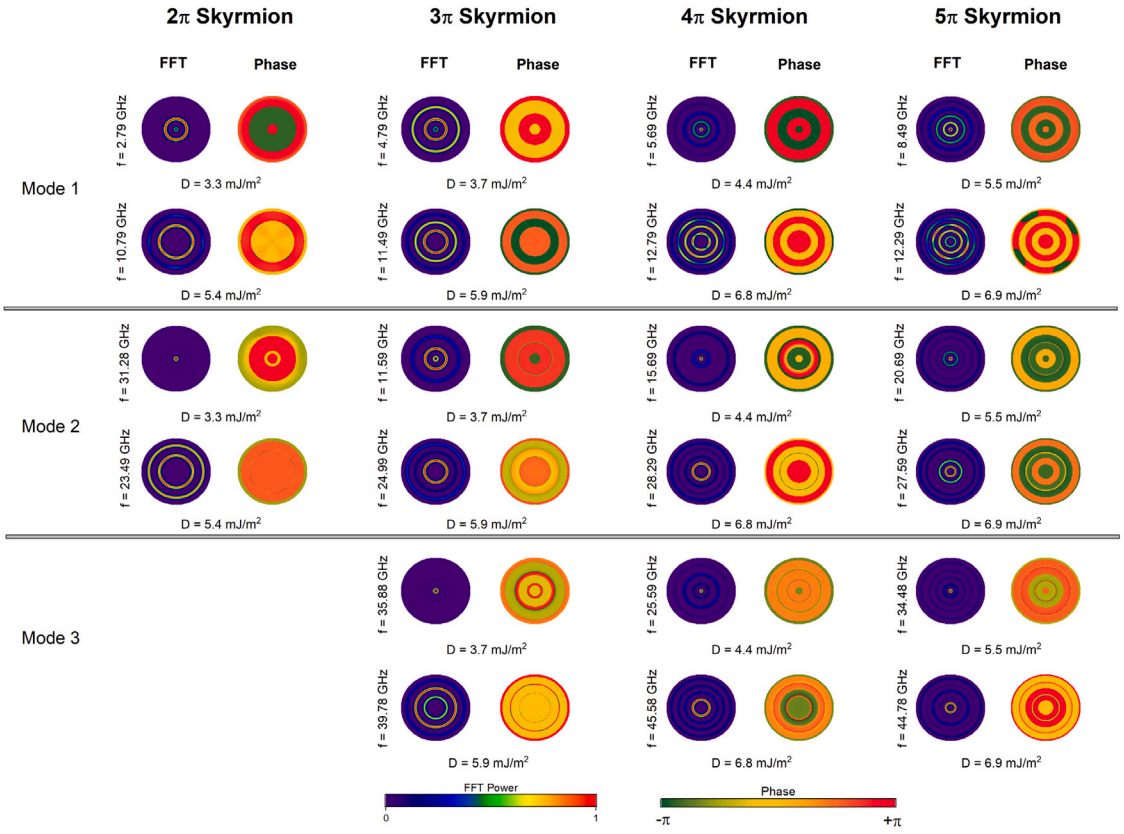

Fig. 4. Spatial distribution profiles of the Fourier power and the phases of the oscillations of the radial spin wave modes as a function of the Dzyaloshinskii–Moriya exchange constant D_{int}.

the small amplitude oscillations, and as D_{int} increases, the diameters of both rings approach the edges of the disk. However, the outer ring increases its oscillation amplitude up to D_{int} = 3.8 mJ/m^2 and then its intensity decreases with the increase of D_{int}, whereas the inner ring increases its intensity with the increase of D_{int}.

For mode 2, initially the maximum amplitude oscillation is distributed in only one ring around the center of the disk and its diameter increases with the increase of D_{int} up to approximately D_{int} = 3.9 mJ/m^2. For higher values of D_{int}, an additional outer ring of small oscillations emerges and both diameters and their amplitudes increase with the increase of D_{int}.

3π skyrmion:

For mode 1, the oscillation amplitudes of the radial spin wave modes are distributed in three rings (outer, middle and inner) around the center of the disk. Initially (D_{int} = 3.3 mJ/m^2) the middle ring has a higher intensity than the other two rings. The diameter and the intensity of the inner ring increase with the increase of D_{int}. The diameter of the middle ring also increases with the increase of D_{int} and keeps its intensity constant up to approximately D_{int} = 4.9 mJ/m^2. For higher values of D_{int}, its intensity decreases gradually. On the other hand, the outer ring decreases its intensity monotonically with the increase of D_{int}.

For mode 2, the oscillation amplitudes of the radial spin wave modes are also distributed in three rings (outer, middle and inner) around the center of the disk. Initially (D_{int} = 3.3 mJ/m^2) the middle ring has a higher intensity than the other two rings. The inner ring increases its intensity and diameter with the increase of D_{int}; the same occurs with the middle ring. However, this ring vanishes for approximately D_{int} = 4.6 mJ/m^2, but it emerges again, for approximately D_{int} = 5.8 mJ/m^2, with a lower intensity, increasing its diameter with the increase of D_{int}. The outer ring increases its diameter and intensity with the increase of D_{int} up to D_{int} = 4.0 mJ/m^2. For higher values of D_{int}, its diameter keeps increasing, but its intensity decreases.

For mode 3, there is only one ring around the center of the nanodisk. Its diameter increases with the increase of D_{int}. On the other hand, its intensity remains constant up to D_{int} = 5.2 mJ/m^2, and then its intensity decreases with the increase of D_{int}. When D_{int} = 4.4 mJ/m^2, another ring emerges of small oscillation amplitude with a larger diameter than that of the first ring. The diameter of this ring increases with the increase of D_{int}, whereas its intensity increases for a maximum value of D_{int} = 5.3 mJ/m^2 and then it remains almost constant. For D_{int} = 5.3 mJ/m^2 an outer ring emerges and it has a lower intensity, and this remains almost constant with the increase of D_{int}, whereas its diameter increases with D_{int}.

4π skyrmion:

For mode 1, the oscillation amplitudes of the radial spin wave modes are distributed in four rings (D_{int} = 4.4 mJ/m^2) around the center of the disk. The larger the diameter, the lower the amplitude of the spin waves, and their diameters increase with the increase of D_{int}. The inner ring has initially a higher intensity when compared with the other rings, but for the next value of D_{int} (D_{int} = 4.5 mJ/m^2), its intensity decreases and its value remains almost constant with the increase of D_{int}. On the other hand, the intensity of the other rings increase their values for D_{int} = 4.5 mJ/m^2 and they remain also constant with the increase of D_{int}.

For mode 2, the oscillation amplitudes are distributed in three rings around the center of the disk. The intensity of each one of them is lower the further away they are from the center. The intensity of the inner ring is kept almost constant with the increases of D_{int}, whereas its diameter increases. The other two rings increase their diameters with the increase of D_{int}, but their intensities decrease.

For mode 3, the oscillation amplitudes are distributed initially in two rings around the center (D_{int} = 3.4 mJ/m^2) . The inner ring has a higher intensity than the other ring. Its intensity remains almost constant, but its diameter increases with the increase of D_{int}. For D_{int} = 3.5 mJ/m^2, there appears a middle ring and its diameter and intensity increase up to D_{int} = 4.7 mJ/m^2 and then the intensity vanishes for higher values of D_{int}. The second ring increases its diameter with the increase of D_{int}, whereas its intensity decreases gradually, vanishing for approximately D_{int} = 6.1 mJ/m^2. From approximately D_{int} = 6.6 mJ/m^2, there appear three extra rings around the center, with lower intensity and their diameters remain constant with the increase of D_{int}.

5π skyrmion:

For mode 1, the oscillation amplitudes are distributed in five rings around the center of the disk. Their diameters increase with the increase of D_{int}, whereas their intensities remain almost constant.

For mode 2, the oscillation amplitudes are also distributed in five rings around the center of the disk. The inner and middle ring have higher intensity in comparison with the outer ring. The diameter and the intensity of the outer ring remain almost constant with the increase of D_{int}, whereas the inner and middle ring increase their diameter, keeping constant their intensities with the increase of D_{int}.

For mode 3, the oscillation amplitudes are distributed in rings around the center of the disk. Their diameters increase with the increase of D_{int}, but their intensities remain almost constant.

In Fig. 4 it is also shown the spatial profile of the phase of the radial spin wave modes. In this figure, we can see that the presence of the Dzyaloshinskii–Moriya interaction leads to a nonuniform phase, due to the nonreciprocity induced by that interaction, resulting in phase jumps along the radial direction. Each ring of spin wave oscillates in its respective phase according to its position in the nanodisk. For example, in mode 1 of the 2π skyrmion, the ring formed by the maximum amplitude of the spin wave oscillates in phase and the ring formed by the lower amplitudes also oscillates in phase.

The power spectra for azimuthal spin wave modes of the kπ skyrmions (k = 2, 3, 4 and 5), as a function of D_{int}, are shown in Fig. Fig. 5. Similarly to the case of the radial spin wave modes, the values of the frequencies of the azimuthal spin wave, in a general way, increase with the increase of D_{int}. The values of those frequencies are shown in the Supplementary Material for the minimum and maximum values of D_{int} where it is possible to obtain the kπ skyrmion. In this stage, in order to determine the direction of rotation of these modes, m = +1 for counterclockwise (CCW) and m = −1 for clockwise (CW) rotation, an in-plane alternating magnetic field, $B_x = B_0 \sin(2\pi ft)$, was used, where f is the frequency of the spin wave mode. The rotation direction is also shown in the Supplementary Material.

In Fig. 6 are shown the spatial profiles of the FFT power and the phase of the azimuthal spin wave modes for a 2π skyrmion. For these modes, the maximum oscillation amplitudes are located in rings around the center of the nanodisk and their diameters increase with the increase of D_{int}. The spatial profiles of the phases of these modes show that the values of the phases change continuously according to their positions in the nanodisk, resulting in spin waves oscillating with different phases. The spatial profile of the FFT power and the phase for the other kπ skyrmions are shown in the Supplementary Material.

As shown in Figs. 3 and 5, the values of the frequencies of the radial and azimuthal modes are strongly influenced by the presence of the DMI interaction. This is due to the fact that it induces a nonreciprocity, which leads to having different wavevectors along specific directions (e.g., in the radial and azimuthal directions). In the case of radial modes, usually considered standing spin waves, the nonreciprocity leads to the existence of waves that are not exactly standing waves. In the case of azimuthal modes, the nonreciprocity is responsible for the frequency splitting of the modes, leading to a counterclockwise and a clockwise rotation modes [36].

We have also studied the evolution of the magnetization and the topological charge under an applied planar magnetic field, for kπ skyrmions. In this stage, a kπ skyrmion (state I in Fig. 7(a–c)) is stabilized in the nanodisk as initial magnetic configuration. After that, an in-plane magnetic field B_x along the x-axis was applied, from 0 up to maximum value of 1.8 T, in 100 mT steps. In each step, the relaxed magnetic state was stored and used as initial state for the next value of magnetic field. The maximum value of the magnetic field employed in this study was not sufficient to saturate the magnetization in the plane.

The magnetic hysteresis curves obtained are shown in Fig. 7(a–c). These loops are different from those obtained with perpendicular magnetic fields (see for example Refs. [37–39]). In that case, the core of the skyrmion expands and shrinks, increasing or decreasing its diameter depending on whether the magnetic field is parallel or antiparallel to the core magnetization. Additionally, there occurs switching of the magnetization, evidenced by sharp jumps in the hysteresis loops [38]. However, in our case the behavior of the magnetization is different (see

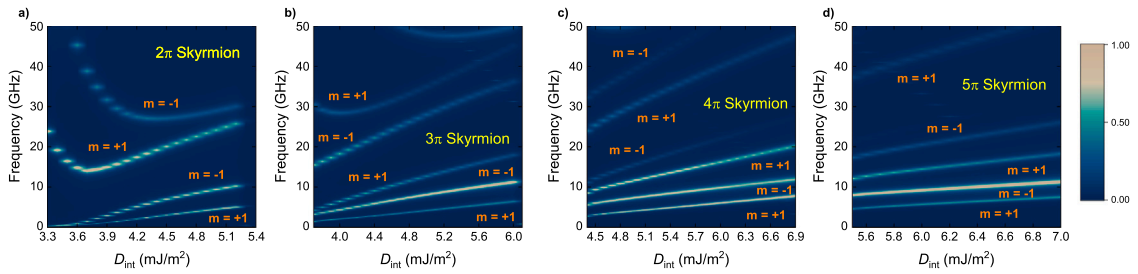

Fig. 5. Power spectra of the kπ skyrmions as a function of the Dzyaloshinskii–Moriya exchange constant D_{int} for azimuthal modes, (a) for a 2π skyrmion, (b) for a 3π skyrmion, (c) for a 4π skyrmion and (c) for a 5π skyrmion.

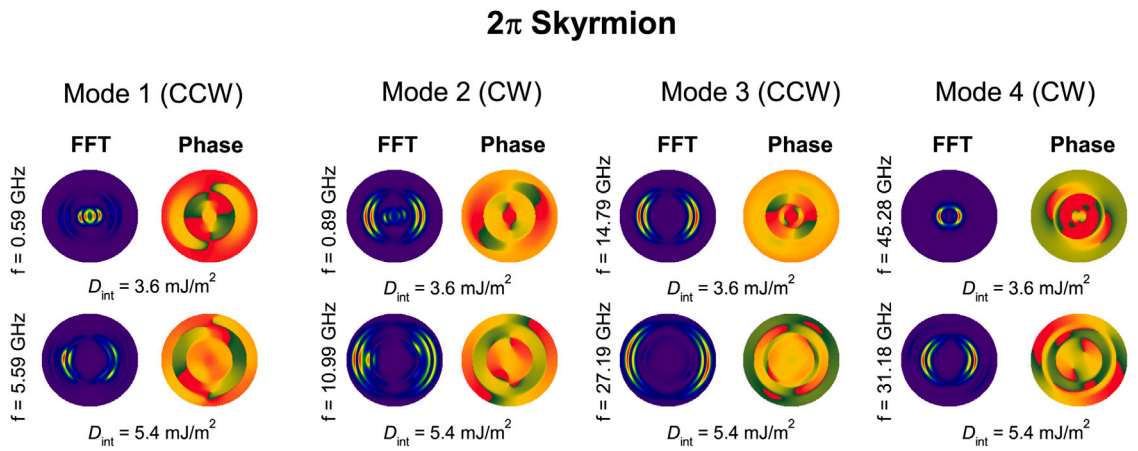

Fig. 6. Spatial distribution profiles of the Fourier power and the phases of the oscillations of the azimuthal spin wave modes as a function of the Dzyaloshinskii–Moriya exchange constant D_{int}, for a 2π skyrmion.

Fig. 7(a–c)) and no switching processes are evident. All the hysteresis loops obtained show small jumps in the evolution of the magnetization, corresponding to changes in the magnetic configuration in the nanodisk. The shape of the core is elongated along the direction of the applied magnetic field (state II in Fig. 7(a)) and its size along this direction increases with the increase of the magnetic field up to the point where the skyrmion is annihilated and a structure with a strange shape appears (state III in Fig. 7(a) and Fig. 7(c) and state II in Fig. 7(b)).

The magnetic hysteresis loops allowed the identification of two types of transitions between skyrmions. In the first type a kπ skyrmion switches to a (k+1)π skyrmion and in the second type a kπ skyrmion collapses to a (k-1)π skyrmion.

In Fig. 7(a–c) are shown the hysteresis loops where the first type of transition appears. For example, in Fig. 7(a) it is shown the hysteresis loop for a 2π skyrmion (D_{int} = 4.5 mJ/m^2) as initial magnetic configuration (state I). Initially, the magnetic moments tend to align with the magnetic field elongating the 2π skyrmion (state II). For a value of B_x = 0.79 T, the elongated 2π skyrmion is annihilated and a new distorted magnetic configuration is created (state III), which is manifest by a jump in the magnetization curve. Distorted magnetic configurations stay in the nanodisk up to the maximum value of the magnetic field (state IV), even when the magnetic field is decreased and it is reversed to negative values (state V). In this part of the magnetic cycle where the fields are negative, a 3π skyrmion is created, for a field of B_x = −0.61 T (state VI). This change in the magnetization is accompanied by another jump in the curve of magnetization. This new skyrmion is annihilated at B_x = −0.85 T and a strange magnetic configuration appears again (small jump in the magnetization curve) and for the negative maximum value of the magnetic field this strange configuration collapses into another (state VII). The 3π skyrmion appears again for a positive value B_x = 0.61 T.

The dependence of the topological charge (Q) on the intensity of magnetic field is also shown in this figure. The values of Q broadly agree with the theoretical values defined for the kπ skyrmions. The jumps in the magnetic hysteresis loop are accompanied by jumps in the values of the topological charge. Similar behaviors are shown in Fig. 7(b–c) for 3π and 4π skyrmion as initial magnetic configuration.[4]

We repeated the same process of analysis of m_x vs. B, and Q vs. B curves, for the whole range of values of D_{int} used in this work. A simplified phase diagram is shown in Fig. 7(d). In this figure we can observe the regions where a transition from a kπ skyrmion to a (k+1)π skyrmion is possible. The diagram also shows regions where it was observed the opposite type of transition, from (k+1)π to a kπ skyrmion. In all cases, the (k+1)π skyrmion is always created when the magnetic fields are negative or when these are increasing from the most negative value, thus it is important to scan almost the complete hysteresis loop. When a 5π skyrmion is used as initial magnetic configuration, it was not possible to obtain a 6π skyrmion. This may be due to two reasons: (a) a 6π skyrmion is not a metastable, or stable state in the nanodisk, or (b) the use of the hysteresis loop may not be suitable for this purpose.

The hysteresis loops for the second type of transitions, i.e., from kπ to (k-1)π skyrmions, can be seen in the Supplementary Material. Those curves show behavior similar to that obtained for the first type of transition.

3. Conclusion

In this work, we have shown that a kπ skyrmion can be stabilized in a ferromagnetic nanodisk tuning parameters such as the

[4] Transitions from a π skyrmion to 2π skyrmion and vice versa are well studied, for example, see Refs. [2,12,15,17].

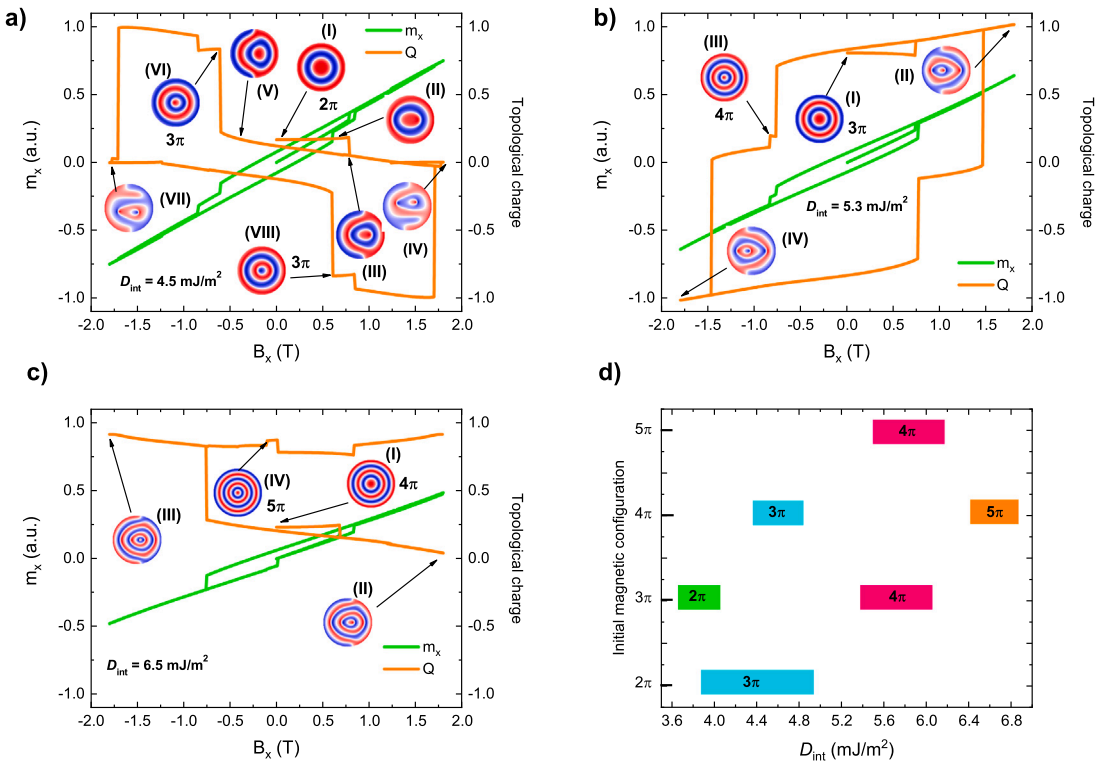

Fig. 7. Hysteresis loops (green curve) and evolution of the topological charge (orange curve) as a function of the planar magnetic field intensity, (a) for a 2π skyrmion, (b) for a 3π skyrmion, (c) for a 4π skyrmion and (d) phase diagram showing the range of values of D_{int} where the corresponding transitions from initial values to final values of $k\pi$ are observed. Note that the diagram contains transitions from $k\pi$ to $(k+1)\pi$ skyrmions, as well as transitions from $(k+1)\pi$ to $k\pi$ skyrmions.

value of the uniaxial perpendicular anisotropy constant K_z and the Dzyaloshinskii–Moriya interaction constant D_{int}.

Our results show that it is even possible to obtain a 4π skyrmion or 5π skyrmion as ground state of the nanodisk. A phase diagram with these results was presented.

We have also shown that the values of the frequencies of the power spectrum and the spatial distributions of the FFT power, for radial and azimuthal spin wave modes, are dependent on the value of D_{int} and the maximum oscillation tends to move towards the edges of the nanodisk when D_{int} increases. These oscillations may be in phase or out of phase.

Our results also show that the switching between a $k\pi$ and a $(k+1)\pi$ skyrmion and vice versa, with a cyclical applied planar magnetic field is possible. This method can be easily implemented experimentally and it is relevant for applications in Spintronics, where a $k\pi$ and a $k'\pi$ skyrmions would represent "0" or "1".

CRediT authorship contribution statement

H. Vigo-Cotrina: Methodology, Software, Writing – original draft. **D.L. Monteiro:** Software. **J.P.V. Urruchua:** Software. **A.P. Guimarães:** Writing – review & editing, Supervision.

Declaration of competing interest

The authors declare that they have no known competing financial interests or personal relationships that could have appeared to influence the work reported in this paper.

Data availability

Data will be made available on request.

Acknowledgments

The authors would like to thank Dr. J.P. Sinnecker for his support during the process of data analysis. The authors would like to acknowledge the support of the Brazilian Agency CNPq.

Appendix A. Supplementary data

Supplementary material related to this article can be found online at https://doi.org/10.1016/j.jmmm.2022.169665.

References

[1] M. Beg, R. Carey, W. Wang, D. Cortés-Ortuño, M. Vousden, M.-A. Bisotti, M. Albert, D. Chernyshenko, O. Hovorka, R.L. Stamps, H. Fangohr, Ground state search, hysteretic behaviour and reversal mechanism of skyrmionic textures in confined helimagnetic nanostructures, Sci. Rep. 5 (1) (2015) 17137, http://dx.doi.org/10.1038/srep17137.

[2] N. Mehmood, R. Fazal, W. Yadong, T. Guo, Q. Zhang, Z. Hou, G. Xingsen, J.-M. Liu, Stability phase diagrams and tuning of magnetic skyrmionium and other states, J. Magn. Magn. Mater. 526 (2021) 167706, http://dx.doi.org/10.1016/j.jmmm.2020.167706.

[3] J. Yang, H.-K. Park, G. Park, C. Abert, D. Suess, S.-K. Kim, Robust formation of skyrmion and skyrmionium in magnetic hemispherical shells and their dynamic switching, Phys. Rev. B 104 (2021) 134427, http://dx.doi.org/10.1103/PhysRevB.104.134427.

[4] L. Bo, L. Kong, R. Zhao, C. Hu, L. Ji, Y. Zhang, X. Zhang, Energy-efficient polarity reversal of a target skyrmion driven by spin-transfer effect, J. Magn. Magn. Mater. 528 (2021) 167705, http://dx.doi.org/10.1016/j.jmmm.2020.167705.

[5] Y. Zhang, C. Xu, P. Chen, Y. Nahas, S. Prokhorenko, L. Bellaiche, Emergence of skyrmionium in a two-dimensional $CrGe(Se,Te)_3$ Janus monolayer, Phys. Rev. B 102 (2020) 241107, http://dx.doi.org/10.1103/PhysRevB.102.241107.

[6] J. Wang, J. Xia, X. Zhang, X. Zheng, G. Li, L. Chen, Y. Zhou, J. Wu, H. Yin, R. Chantrell, Y. Xu, Magnetic skyrmionium diode with a magnetic anisotropy voltage gating, Appl. Phys. Lett. 117 (20) (2020) 202401, http://dx.doi.org/10.1063/5.0025124.

[7] C. Moutafis, S. Komineas, C.A.F. Vaz, J.A.C. Bland, T. Shima, T. Seki, K. Takanashi, Magnetic bubbles in FePt nanodots with perpendicular anisotropy, Phys. Rev. B 76 (2007) 104426, http://dx.doi.org/10.1103/PhysRevB.76.104426.

[8] D. Cortés-Ortuño, N. Romming, M. Beg, K. von Bergmann, A. Kubetzka, O. Hovorka, H. Fangohr, R. Wiesendanger, Nanoscale magnetic skyrmions and target states in confined geometries, Phys. Rev. B 99 (2019) 214408, http://dx.doi.org/10.1103/PhysRevB.99.214408.

[9] B. Göbel, I. Mertig, O.A. Tretiakov, Beyond skyrmions: Review and perspectives of alternative magnetic quasiparticles, Phys. Rep. 895 (2021) 1–28, http://dx.doi.org/10.1016/j.physrep.2020.10.001.

[10] S.K. Panigrahy, C. Singh, A.K. Nayak, Current-induced nucleation, manipulation, and reversible switching of antiskyrmioniums, Appl. Phys. Lett. 115 (18) (2019) 182403, http://dx.doi.org/10.1063/1.5125290.

[11] A.G. Kolesnikov, M.E. Stebliy, A.S. Samardak, A.V. Ognev, Skyrmionium – High velocity without the skyrmion Hall effect, Sci. Rep. 8 (1) (2018) 16966, http://dx.doi.org/10.1038/s41598-018-34934-2.

[12] X. Zhang, J. Xia, Y. Zhou, D. Wang, X. Liu, W. Zhao, M. Ezawa, Control and manipulation of a magnetic skyrmionium in nanostructures, Phys. Rev. B 94 (2016) 094420, http://dx.doi.org/10.1103/PhysRevB.94.094420.

[13] J. Sampaio, V. Cros, S. Rohart, A. Thiaville, A. Fert, Nucleation, stability and current-induced motion of isolated magnetic skyrmions in nanostructures, Nature Nanotechnology 8 (2013) 839–844, http://dx.doi.org/10.1038/nnano.2013.210.

[14] N. Vidal-Silva, A. Riveros, J. Escrig, Stability of Neel Skyrmions in ultra-thin nanodots considering Dzyaloshinskii–Moriya and dipolar interactions, J. Magn. Magn. Mater. 443 (2017) 116–123, http://dx.doi.org/10.1016/j.jmmm.2017.07.049.

[15] Y. Ishida, K. Kondo, Theoretical comparison between skyrmion and skyrmionium motions for spintronics applications, 59 (SG) (2020) 04, http://dx.doi.org/10.7567/1347-4065/ab5b6b.

[16] A. Mahmoud, F. Ciubotaru, F. Vanderveken, A.V. Chumak, S. Hamdioui, C. Adelmann, S. Cotofana, Introduction to spin wave computing, J. Appl. Phys. 128 (16) (2020) 161101, http://dx.doi.org/10.1063/5.0019328.

[17] H. Vigo-Cotrina, A.P. Guimarães, Creating skyrmions and skyrmioniums using oscillating perpendicular magnetic fields, J. Magn. Magn. Mater. 507 (2020) 166848, http://dx.doi.org/10.1016/j.jmmm.2020.166848.

[18] H. Vigo-Cotrina, A.P. Guimarães, Switching of skyrmioniums induced by oscillating magnetic field pulses, J. Magn. Magn. Mater. 509 (2020) 166895, http://dx.doi.org/10.1016/j.jmmm.2020.166895.

[19] B. Zhang, W. Wang, M. Beg, H. Fangohr, W. Kuch, Microwave-induced dynamic switching of magnetic skyrmion cores in nanodots, Appl. Phys. Lett. 106 (10) (2015) 102401, http://dx.doi.org/10.1063/1.4914496.

[20] M. Shen, Y. Zhang, J. Ou-Yang, X. Yang, L. You, Motion of a skyrmionium driven by spin wave, Appl. Phys. Lett. 112 (6) (2018) 062403, http://dx.doi.org/10.1063/1.5010605.

[21] R. Zhao, C. Hu, L. Ji, W. Chen, X. Zhang, Persistent excitation of spin waves for kπ-state skyrmions, Sci. China Phys. Mech. Astron. 63 (6) (2020) 267511, http://dx.doi.org/10.1007/s11433-020-1529-0.

[22] Y. Liu, G. Yin, J. Zang, J. Shi, R.K. Lake, Skyrmion creation and annihilation by spin waves, Appl. Phys. Lett. 107 (15) (2015) 152411, http://dx.doi.org/10.1063/1.4933407.

[23] J.-V. Kim, F. Garcia-Sanchez, J.a. Sampaio, C. Moreau-Luchaire, V. Cros, A. Fert, Breathing modes of confined skyrmions in ultrathin magnetic dots, Phys. Rev. B 90 (2014) 064410, http://dx.doi.org/10.1103/PhysRevB.90.064410.

[24] M. Lonsky, A. Hoffmann, Coupled skyrmion breathing modes in synthetic ferri- and antiferromagnets, Phys. Rev. B 102 (2020) 104403, http://dx.doi.org/10.1103/PhysRevB.102.104403.

[25] Y. Liu, R.K. Lake, J. Zang, Shape dependent resonant modes of skyrmions in magnetic nanodisks, J. Magn. Magn. Mater. 455 (2018) 9–13, Magnetic skyrmions as future information carriers.

[26] V.P.K. Miriyala, Z. Zhu, G. Liang, X. Fong, Spin-wave mediated interactions for majority computation using skyrmions and spin-torque nano-oscillators, J. Magn. Magn. Mater. 486 (2019) 165271, http://dx.doi.org/10.1016/j.jmmm.2019.165271.

[27] C. Song, Y. Ma, C. Jin, J. Wang, H. Xia, J. Wang, Q. Liu, Field-tuned spin excitation spectrum of kπ skyrmion, New J. Phys. 21 (8) (2019) 083006, http://dx.doi.org/10.1088/1367-2630/ab348e.

[28] X. Liu, Q. Zhu, S. Zhang, Q. Liu, J. Wang, Static property and current-driven precession of 2kπ-vortex in nano-disk with Dzyaloshinskii–Moriya interaction, AIP Adv. 5 (8) (2015) 087137, http://dx.doi.org/10.1063/1.4928727.

[29] N. Mehmood, X. Song, G. Tian, Z. Hou, D. Chen, Z. Fan, M. Qin, X. Gao, J.-M. Liu, Strain-mediated electric manipulation of magnetic skyrmion and other topological states in geometric confined nanodiscs, J. Phys. D: Appl. Phys. 53 (1) (2019) 014007, http://dx.doi.org/10.1088/1361-6463/ab47bd.

[30] A. Vansteenkiste, J. Leliaert, M. Dvornik, M. Helsen, F. Garcia-Sanchez, B. Van Waeyenberge, The design and verification of MuMax3, AIP Adv. 4 (10) (2014) 107133, http://dx.doi.org/10.1063/1.4899186.

[31] H. Yang, A. Thiaville, S. Rohart, A. Fert, M. Chshiev, Anatomy of Dzyaloshinskii–Moriya interaction at Co/Pt interfaces, Phys. Rev. Lett. 115 (2015) 267210, http://dx.doi.org/10.1103/PhysRevLett.115.267210.

[32] H. Yang, O. Boulle, V. Cros, A. Fert, M. Chshiev, Controlling Dzyaloshinskii–Moriya interaction via chirality dependent atomic-layer stacking, insulator capping and electric field, Sci. Rep. 8 (1) (2018) 12356, http://dx.doi.org/10.1038/s41598-018-30063-y.

[33] E. Simon, L. Rózsa, K. Palotás, L. Szunyogh, Magnetism of a Co monolayer on Pt(111) capped by overlayers of 5*d* elements: A spin-model study, Phys. Rev. B 97 (2018) 134405, http://dx.doi.org/10.1103/PhysRevB.97.134405.

[34] A. Cao, X. Zhang, B. Koopmans, S. Peng, Y. Zhang, Z. Wang, S. Yan, H. Yang, W. Zhao, Tuning the Dzyaloshinskii–Moriya interaction in Pt/Co/MgO heterostructures through the MgO thickness, Nanoscale 10 (2018) 12062–12067, http://dx.doi.org/10.1039/C7NR08085A.

[35] M. Mruczkiewicz, P. Gruszecki, M. Krawczyk, K.Y. Guslienko, Azimuthal spin-wave excitations in magnetic nanodots over the soliton background: Vortex, Bloch, and Néel-like skyrmions, Phys. Rev. B 97 (2018) 064418, http://dx.doi.org/10.1103/PhysRevB.97.064418.

[36] F. Garcia-Sanchez, P. Borys, A. Vansteenkiste, J.-V. Kim, R.L. Stamps, Non-reciprocal spin-wave channeling along textures driven by the Dzyaloshinskii–Moriya interaction, Phys. Rev. B 89 (2014) 224408, http://dx.doi.org/10.1103/PhysRevB.89.224408.

[37] K. Zeissler, M. Mruczkiewicz, S. Finizio, J. Raabe, P.M. Shepley, A.V. Sadovnikov, S.A. Nikitov, K. Fallon, S. McFadzean, S. McVitie, T.A. Moore, G. Burnell, C.H. Marrows, Pinning and hysteresis in the field dependent diameter evolution of skyrmions in Pt/Co/Ir superlattice stacks, Sci. Rep. 7 (1) (2017) 15125.

[38] A. Talapatra, J. Mohanty, Scalable magnetic skyrmions in nanostructures, Comput. Mater. Sci. 154 (2018) 481–487, http://dx.doi.org/10.1016/j.commatsci.2018.08.022.

[39] J. Brandão, D.A. Dugato, R.L. Seeger, J.C. Denardin, T.J.A. Mori, J.C. Cezar, Observation of magnetic skyrmions in unpatterned symmetric multilayers at room temperature and zero magnetic field, Sci. Rep. 9 (1) (2019) 4144, http://dx.doi.org/10.1038/s41598-019-40705-4.